Journal of Nuclear Materials 609 (2025) 155758

Contents lists available at ScienceDirect

Journal of Nuclear Materials

journal homepage: www.elsevier.com/locate/jnucmat

# Computational analysis of plasma-wall interactions in beryllium: A detailed study of physical and chemically assisted physical sputtering

Nima Fakhrayi Mofrad [a,*], Juri Romazanov [b], Roy Schumacher [a], Andrea E. Sand [a]

[a] Department of Applied Physics, Aalto University, 00076, Espoo, Finland
[b] Institut für Energie und Klimaforschung, Forschungszentrum Jülich, Jülich, Germany

ARTICLE INFO

*Keywords:*
Plasma-wall interaction
Beryllium
Physical sputtering
Chemically assisted physical sputtering
Molecular dynamics

ABSTRACT

Understanding plasma-wall interactions is one of the main challenges in the design and development of fusion reactors. Among the primary effects of these interactions is the erosion of plasma-facing components through physical or chemical sputtering, which can limit the availability and performance of the device. We simulate this phenomenon in beryllium surfaces with varying concentrations of hydrogen isotopes using atomistic molecular dynamics. Special attention is given to chemical sputtering and the overall behavior of molecules emitted from the surface. Our findings indicate that the balance between physical and chemical sputtering is considerably affected by isotope type, impact energy, and incident angle of the plasma particle. We compare the results with predictions from SDTrimSP, a tool that utilizes the more computationally efficient binary collision approximation, to elucidate the conditions where the higher accuracy of molecular dynamics is needed. Moreover, we highlight the effect of surface temperature, which determines the concentration of hydrogen isotopes in the surface layers, on the contribution of chemical sputtering to total erosion, and the types of sputtered molecules. Lastly, we demonstrate that the escape energies and angles of the sputtered species are also significantly influenced by the impact energy and angle of the plasma particles.

## 1. Introduction

With the growing concern about global warming and the increasing energy demand, the need for sustainable energy sources is becoming a necessity. Fusion can offer an environmentally friendly alternative to traditional energy sources, without greenhouse gases as by-products. However, there are some challenges to overcome to have a fully operational fusion reactor. Understanding plasma-wall interactions (PWIs) and their effects is one of the main obstacles.

One effect of the interactions with energetic particles from the plasma is the erosion of plasma-facing components (PFCs) by physical sputtering, and by chemically assisted physical sputtering (CAPS). There is also thermally activated erosion, *i.e.* chemical erosion, which is significant in carbon-based materials [1]. In this process, the impact of hydrogen on carbon surfaces results in the formation of a radical intermediate. At temperatures exceeding 400 K, this intermediate can undergo erosion, leading to the detachment of a methyl group [2]. However, the phenomenon of chemical erosion is not a subject addressed in this study.

Both the plasma performance and the life time and availability of the reactor are highly dependent on the rate of erosion and the characteristics of eroded species. Furthermore, redeposition of sputtered impurities is one of the main contributors to tritium retention, which is a major concern in fusion reactors [3,4]. These effects necessitate significant focus on the investigation of the sputtering process.

Physical sputtering occurs when the energy transferred from the incident ion to the target atom exceeds the surface bonding energy [5]. Therefore, physical sputtering requires a minimum energy transfer of approximately 1-9 eV to the target atoms [6], suggesting that the ion energy must be considerably higher. For example, the threshold energy for hydrogen isotopes to cause physical sputtering in carbon-based materials is about 30 eV [7]. Accordingly, one could expect that for ion energies lower than this threshold value, the sputtering yield should be negligible if not zero. However, much higher sputtering yields (on the order of $10^{-2}$) were measured from these materials at room temperature, when irradiated by 10 eV hydrogen ions [8]. The authors note that the high yields cannot be attributed to chemical erosion under these low-temperature, low-energy conditions, implying the presence of an alternative mechanism.

* Corresponding author.
*E-mail address:* nima.fakhrayimofrad@aalto.fi (N. Fakhrayi Mofrad).

https://doi.org/10.1016/j.jnucmat.2025.155758
Received 8 November 2024; Received in revised form 13 March 2025; Accepted 16 March 2025

Available online 20 March 2025

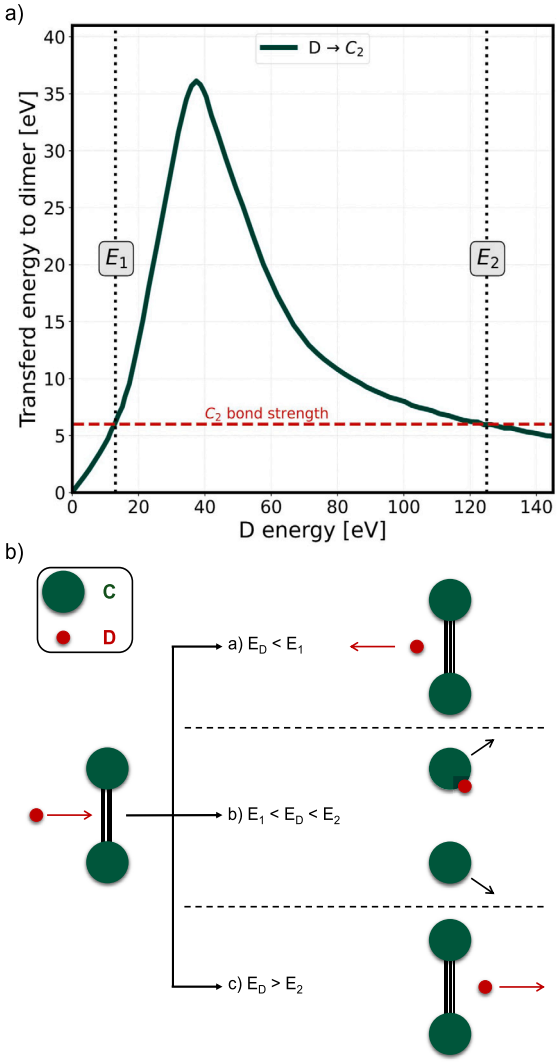


**Fig. 1.** Illustration of a) energy transfer between a D ion and a carbon dimer and b) energy dependence of CAPS bond breaking in a carbon dimer, adapted from the reference [9,11]. (For interpretation of the colors in the figure(s), the reader is referred to the web version of this article.)

Molecular dynamics (MD) simulations were employed to determine the primary cause of the significant erosion rates seen when carbon is irradiated by low-energy hydrogen ions. As a result, the CAPS mechanism (also known as "swift chemical sputtering") was identified, a process during which the incoming hydrogen ion spends sufficient time in the bonding region between two carbon atoms to chemically break their bond, leading to sputtering (Fig. 1-b, Panel b) [9,10]. For this mechanism to occur, the momentum, *i.e.*, energy of the projectile, as well as the duration it interacts within the bonding region, must be sufficient. If the energy is too low, the projectile cannot penetrate the bonding region and will be reflected (Fig. 1-b, Panel a). In contrast, if the energy is too high, the projectile will enter the bonding region but the interaction time is too short for breaking the bond between the two target atoms (Fig. 1-b, Panel c). This introduces a certain energy range, in which CAPS will contribute noticeably to total erosion. For example, in carbon-based materials irradiated by deuterium, this energy range is about 10-130 eV. This explains the high sputtering yields at low energies observed in previous experiments. Furthermore, while CAPS is especially prominent in carbon, it can also occur in other materials [11,12]. Moreover, it is important to note that in experiments, CAPS is characterized by spectroscopically observing molecular sputtering via the photon emissions from the sputtered species [13]. Consequently, the term CAPS, as used in this context, refers to molecular sputtering.

Despite many attempts to predict molecular sputtering and its effect on reactor performance, there are still several unknowns in this area. These include the characteristics of different molecules released from the surface of PFCs, the effect of energy and angle of the incoming ion on CAPS, and the impact of different plasma particles on the contribution of CAPS to the total erosion [14,15]. To address these issues, our study concentrates on beryllium (Be), for which a large body of experimental data has been obtained from JET, and where the presence of CAPS is confirmed [13,16]. Be has been one of the choices for the first wall armor in ITER, because of its low atomic number and high affinity for oxygen. These characteristics are helpful in keeping the plasma clean and preventing energy loss [17]. Although focus is now shifted to boron-coated tungsten as a plasma-facing material [18], in order to lower tritium retention and dust production, investigating Be remains important for assessing the sputtering mechanisms. This is particularly pertinent in light of the available experimental data concerning CAPS and the subsequent behavior of the sputtered molecular species within the plasma, since molecular sputtering is also present in other fusion relevant materials, including boron and tungsten [19–21].

This study presents simulations on the irradiation of various Be surfaces by hydrogen (H), deuterium (D), and tritium (T) plasma particles. The aim is to evaluate the effects of different parameters, including impact energy, isotope type, incident angle, and surface temperature, with high fidelity. Consequently, this work offers important insight on erosion and specifically the contribution of molecular sputtering to the total sputtering yield, and provides input for large-scale impurity transport codes such as ERO [22].

## 2. Model and simulation details

### 2.1. Molecular dynamics

MD simulation is a commonly used numerical method that predicts the motions of atoms subject to forces computed from interatomic potentials. Utilizing an accurate potential turns MD into an exceptionally effective tool for investigating PWIs in fusion reactors. In this study, the irradiation of Be surfaces was modeled with the LAMMPS code [23], using a many-body bond-order Tersoff/ZBL potential developed specifically for studies of plasma particle interactions with surfaces [24]. There are two versions of this potential, and we have utilized the first version, given that the second variant is designed to address interactions involving carbon atoms and does not predict certain properties of bulk Be as accurately as the first version (refer to the supporting information for more details). The following sections present a detailed explanation of the different steps involved in the simulation process.

#### 2.1.1. Surface preparation

As a first step, surfaces were prepared with an appropriate concentration of hydrogen isotopes (H/D/T) for different surface temperatures. To achieve this, we utilized the density profiles derived by Safi et al. using the object kinetic Monte Carlo (OKMC) technique [25].

Initially, we created a hexagonal closed-packed structure of Be consisting of 3888 atoms with cell dimensions of $x = 2.1$ nm, $y = 2.4$ nm, and $z = 6.4$ nm (Fig. 2, panel a), using the Atomsk program [26]. Then, we randomly removed 7% of the Be atoms to generate vacancies in the structure (Fig. 2, panel b). Subsequently, we selected a certain number of vacancies in each depth range and inserted five hydrogen isotopes in each vacancy to obtain the desired density profiles (Fig. 2, panel c). This decision was supported by the confirmed presence of five deuterium atoms in the Be monovacancy through OKMC and density functional theory (DFT) calculations [25].

Next, we equilibrated the cells for 30 ps with the isothermal-isobaric (NPT) ensemble at the required temperature and zero bar using the

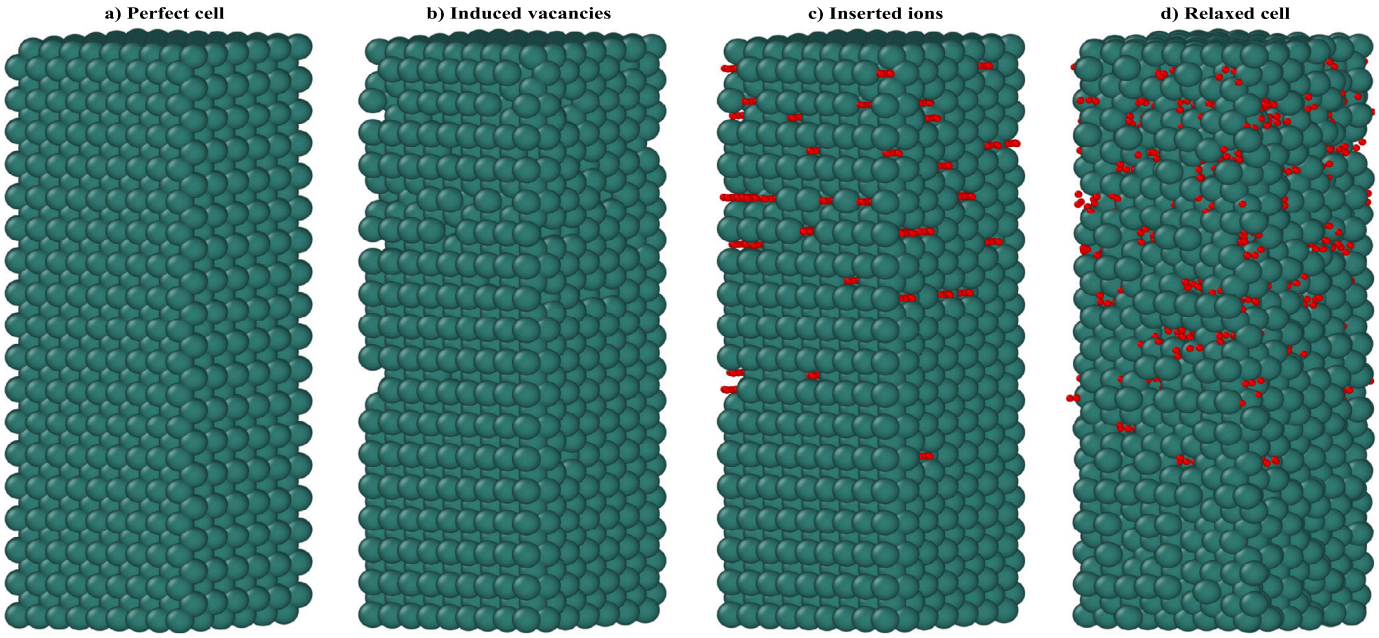


**Fig. 2.** Schematic of different states in the Be-H/D/T surface preparation process, visualized by OVITO [27] software.

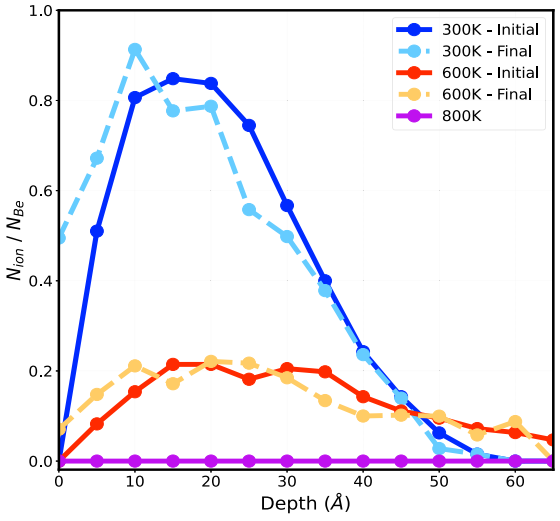


**Fig. 3.** Initial and final hydrogen isotope distribution in Be-H/D/T surfaces with 7% vacancy at different temperatures.

Berendsen temperature and pressure control [28], with periodic boundary condition (PBC) in all directions. Then, we opened the (0001) surface (in the $z$ direction) and relaxed each cell further for another 30 ps. For this relaxation the canonical (NVE) ensemble was used, with PBC in the $x$ and $y$ directions and a fixed bottom layer in the $z$ direction (see Fig. 2 panel d for the final structure). At 800 K the concentration of hydrogen isotopes in the surface layers is predicted to be zero. Therefore, at this temperature, the cells were equilibrated after generating the vacancies, without inserting any hydrogen isotopes. Fig. 3 shows the initial (before relaxation) and final (after relaxation) density profiles at each temperature. Furthermore, the perfect Be cell (Fig. 2, panel a) was also equilibrated in the same way and was used in some cases to better understand how vacancies and hydrogen isotope concentration influence molecular sputtering.

Moreover, in the Supporting Information, we show that a minor alteration in the arrangement of hydrogen isotopes in the surface layer does not have a significant impact on the results. This verifies the statistical credibility of the results obtained by employing one surface for each scenario.

**Table 1**
Size of the cell used in each irradiation simulation regardless of surface temperature.

| Impact energy [eV] | Normal incidence | Angled incidence |
|---|---|---|
| E < 50 | 1×1 Cell | 2×2 Cell |
| 50 ≤ E < 150 | 2×2 Cell | 3×3 Cell |
| 150 ≤ E | 3×3 Cell | 3×3 Cell |

### 2.1.2. Cell size

During the irradiation simulations, the temperature of the system was controlled by applying a Berendsen thermostat on the cell borders, as explained in detail by K. Vörtler et al. [29]. This implementation serves as a mechanism for damping the elastic waves in the structure, similar to what happens in bulk materials, enabling a more realistic simulation of the irradiation process. However, if the inbound plasma particle enters this temperature control region, as noted in some of our preliminarily high energy simulations, it will lose its energy to the thermostat, which could reduce the sputtering yield artificially. To prevent this from occurring with more energetic incoming ions, we prepared two additional cells by replicating the obtained cells 2 and 3 times in both the $x$ and $y$ directions. The new cells were then relaxed for 15 ps to make sure that the energy of the system was minimized. Table 1 outlines the cell sizes used for each simulation setup.

### 2.1.3. Time step

The time step for the irradiation simulations is dynamically adjusted based on the velocity of the particles. This is achieved in LAMMPS by indicating the maximum allowed time interval ($dt$) and the maximum distance ($dx$) that each particle is allowed to move in one step. These values need to be selected carefully to ensure the reliability of the results.

To determine the suitable setting for the time step, we performed a set of irradiation simulations with different values for maximum $dt$ and $dx$. In these simulations, no thermostat and electronic stopping were employed to prevent energy dissipation. This allows us to capture the effect of time step on the energy conservation. Consequently, the best

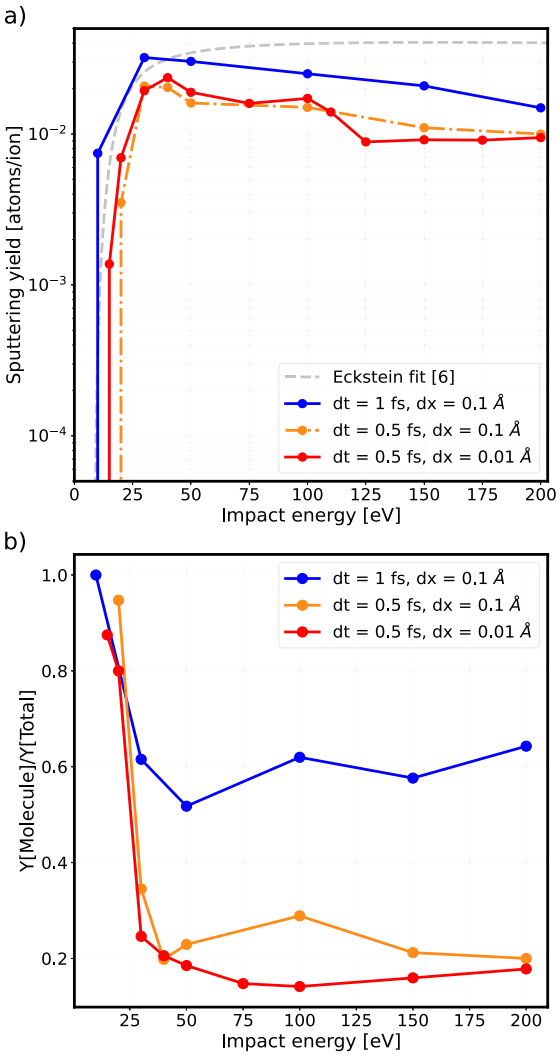


**Fig. 4.** Effect of time step on a) the sputtering yield and b) molecular sputtering in Be-D structures. The grey dashed line represents the Eckstein formula for sputtering [6].

**Table 2**
Fitting values for the Eckstein formula.

| Ion | Target | $\lambda$ | q | $\mu$ | $E_{th}$ (eV) |
|---|---|---|---|---|---|
| H | Be | 0.8007 | 0.0564 | 1.5147 | 14.340 |
| D | Be | 1.7575 | 0.1044 | 1.9906 | 9.5059 |
| T | Be | 2.0794 | 0.1379 | 1.5660 | 9.4345 |

combination for $dt$ and $dx$ would be the one that preserves the energy more accurately while still being computationally feasible. In our systems, we identified a combination of $dt = 0.5$ fs and $dx = 0.01$ Å as the optimal setting for energy conservation, resulting in an energy change ($\Delta E$) of $4 \times 10^{-5}$ eV per atom (Supporting Information, Fig. S4).

The effect of time step on total sputtering and molecular sputtering predictions of the Be-D structure is shown in Fig. 4. The gray dashed line depicted in panel a represents the Eckstein formula for the sputtering yield at normal incidence (Supporting Information, Equations 1-4) with values for the parameters given in Table 2, as referenced in [6].

It can be seen that reducing the time step results in a lower sputtering yield in the structure (Fig. 4, panel a). Furthermore, reducing the time step will noticeably reduce the ratio of sputtered molecules to total sputtered species (Fig. 4, panel b). These findings suggest that the presence of hydrogen isotopes and the predictions of molecular sputtering set high requirements for the accuracy of the irradiation simulations. If the time step of the simulations is too large, it compromises energy conservation, leading to inaccuracies in the trajectories of atoms, and this has a greater influence on hydrogen isotopes. This is because these particles are significantly lighter than the Be target atoms and therefore move at a much higher speed. As can be seen in Fig. S4, this inadequate energy conservation due to a large $dt$ or $dx$ persists throughout the simulation, even after initial impact and slowing of the projectile. This leads to excessive molecular yields, as molecular sputtering is much slower than physical sputtering, occurring well after the initial impact. We attribute the higher molecular yields with high $dt$ or $dx$ to simulation artifacts, since improved energy conservation reduces yield. Therefore, employing a smaller time step enhances the accuracy of the result by stabilizing the MD trajectory and using finer integration intervals [30].

After preparing the Be-H, Be-D, and Be-T structures and selecting the appropriate time step and cell size, we carried out a certain number of non-cumulative impact simulations on each surface as indicated in Table 3, varying the impact energy (10 - 300 eV), surface temperature (300, 600, and 800 K), and incident angle (0 - 75 degrees). Furthermore, the impact point was varied in each simulation by randomly shifting the cell in the $x$ and $y$ directions, to uniformly sample the variations in the surface.

### 2.2. SDTrimSP

The binary collision approximation (BCA) is a widely used Monte Carlo method in the study of radiation damage. Notable programs utilizing the BCA model include TRIM [31], TRIDYN [32], and SDTrimSP [33]. In this work, we employed SDTrimSP to model the sputtering yield of Be structures containing pre-existing hydrogen isotope concentrations, analogous to those used in the MD simulations. However, it should be noted that the SDTrimSP version employed here (version 6.0) is tailored to simulate atomic collisions within amorphous targets, while our MD simulations incorporate the crystalline structure of Be.

We set the concentration of the hydrogen isotope in the sample to 50%, to match the ~ 1:1 ratio between the hydrogen isotope and the target atom in the MD simulations at 300 K. In addition, SDTrimSP requires multiple essential input variables to perform the calculations. First, there is the interaction potential, for which we employed the Krypton-Carbon potential (a repulsive potential with a Moliere-like form) [34]. This potential performs well under a wide range of conditions, including the sputtering of Be by hydrogen [33,35]. Next, we set the surface binding model for the simulations. For this, we selected the model implemented in SDTrimSP which uses the surface binding energy of each individual element within the compound, where the binding energy is independent of the composition of the surface. This model shows good performance in predicting the sputtering yield of different materials by light ions [33]. Moreover, all simulations utilized parameters from the standard SDTrimSP tables as presented in Table 4. We performed the simulations in static mode, where every projectile will interact with the identical predefined surface, making the condition similar to our non-cumulative MD simulations.

## 3. Results and discussion

### 3.1. Sputtering yield

Fig. 5 compares the sputtering yield predicted for the Be-D structure by our MD and SDTrimSP simulations at 300 K for normal D incidence, with data presented in the literature. The results of our MD simulations are in line with the experimental data of plasma-deposited Be layers with D present in the layer [36]. Furthermore, there is also good agreement at low energies with other MD simulations on Be [13,37].

At high impact energies, the SDTrimSP results agree well with the MD predictions. However, at low impact energies, a significant discrepancy in yields is observed. This difference comes from the predominance

**Table 3**
Summary of the Systems, Simulation Parameters, and number of simulations performed.

| System | T [K] | Impact energy [eV] | Impact angle [deg] | No. of simulations |
|---|---|---|---|---|
| Prefect | 300 | 10, 20, 30, 40, 50 | 0 | 3000 |
| Be | 300 | 100, 150, 200 | 0 | 8000 |
| | 300 | 30, 40, 100, 150, 200 | 0 | 3000 |
| | 300 | 10, 15, 20, 25, 50, 75 | 0 | 6000 |
| | 300 | 10, 15, 20, 30, 40, 50, 200, 300 | 40 | 3000 |
| Be-H | 300 | 100, 150 | 40 | 6000 |
| | 300 | 100 | 10, 20, 50, 60, 65, 70, 75 | 3000 |
| | 300 | 100 | 30 | 9000 |
| | 600, 800 | all | 0 | 3000 |
| | 300 | 10, 110 | 0 | 3000 |
| | 300 | 15, 20, 40, 50, 125, 175 | 0 | 6000 |
| | 300 | 100, 150, 200 | 0 | 8000 |
| | 300 | 75 | 0 | 8000 |
| | 300 | 30 | 0 | 10000 |
| Be-D | 300 | 10, 20,30, 100, 150, 200, 300 | 40 | 3000 |
| | 300 | 40, 50 | 40 | 6000 |
| | 300 | 100 | 10 | 9000 |
| | 300 | 100 | 20, 50, 55, 60, 70, 75 | 3000 |
| | 300 | 100 | 30, 65, 67.5 | 6000 |
| | 600, 800 | 10, 20, 30, 40, 50 | 0 | 3000 |
| | 600, 800 | 100, 150, 200 | 0 | 9000 |
| | 300 | 10, 15, 30, 40, 50, 100, 150, 200 | 0 | 3000 |
| | 300 | 20, 60, 75 | 0 | 6000 |
| | 300 | 10, 15, 20, 25, 30, 40, 50, 75, 100, 300 | 40 | 3000 |
| Be-T | 300 | 150, 200 | 40 | 6000 |
| | 300 | 100 | 10, 30, 50, 60, 65, 70, 75 | 3000 |
| | 300 | 100 | 20 | 6000 |
| | 600, 800 | all | 0 | 3000 |

**Table 4**
Values of surface binding energy ($E_{sb}$), displacement energy ($E_d$), bulk binding energy ($E_b$), and cutoff energy in SDTrimSP simulations.

| Atom | $E_{sb}$ [eV] | $E_d$ [eV] | $E_b$ [eV] | Cutoff energy [eV] |
|---|---|---|---|---|
| Be | 3.31 | 15.0 | 0.0 | 3.0 |
| H | 1.10 | 5.0 | 0.0 | 1.0 |
| D | 1.10 | 10.0 | 0.0 | 1.0 |
| T | 1.10 | 15.0 | 0.0 | 1.0 |

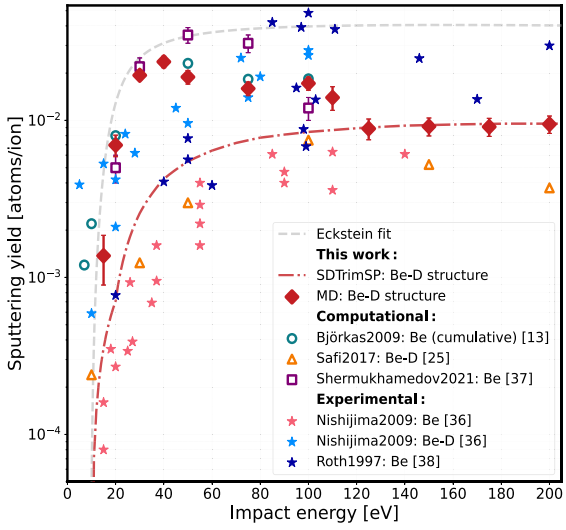


**Fig. 5.** Total sputtering yield by D irradiations as a function of impact energy at 300 K. Experimental values are from Nishijima2009 [36] and from Roth1997 [38]. Computational values are taken from Björkas2009 [13], Safi2017 [25], and Shermukhamedov2021 [37].

of molecular sputtering at low energies, which SDTrimSP fails to capture [39]. Consequently, the yield derived from MD is substantially greater than that given by SDTrimSP. These findings imply the importance of performing MD simulations, especially at low energies, where sputtering is not purely physical.

The effect of isotope type, incident angle, and surface temperature on the sputtering yield of Be structures is discussed in detail in the following sections.

### 3.1.1. Isotope type

As explained, physical sputtering occurs when the amount of energy transferred from the impinging ion to the target atom is sufficient to overcome the surface binding energy. Moreover, the maximum energy ($T_m$) that the ion can transfer to the target atom is [31]:

$$T_m = \frac{4m_1 m_2}{(m_1 + m_2)^2} \times E \tag{1}$$

where $m_1$ and $m_2$ are the masses of the ion and the target atom, respectively, and $E$ is the energy of the ion. Therefore, in case of the Be target atoms, $T_m$ is 36.18%, 59.71%, and 75.14% of the H, D, and T initial energy, respectively. This indicates that increasing the mass of the projectile will increase the amount of energy transferred to the target atom, which in turn should increase the sputtering yield.

Fig. 6 displays the sputtering yield of Be-H, Be-D, and Be-T structures at 300 K for normal and 40-degree incidence by H, D, and T plasma particles.

Going from H to T, the sputtering yield increases for both incident angles as expected. Furthermore, there is good agreement between the MD results for the Be-D structure at 40 degrees and the experimental values for pure Be at 45 degrees (triangles in Fig. 6, panel b). Moreover, for both incident angles, the same trend can be observed in the comparison between the MD and SDTrimSP results of all isotopes, with poor agreement at low energies and good agreement at high energies.

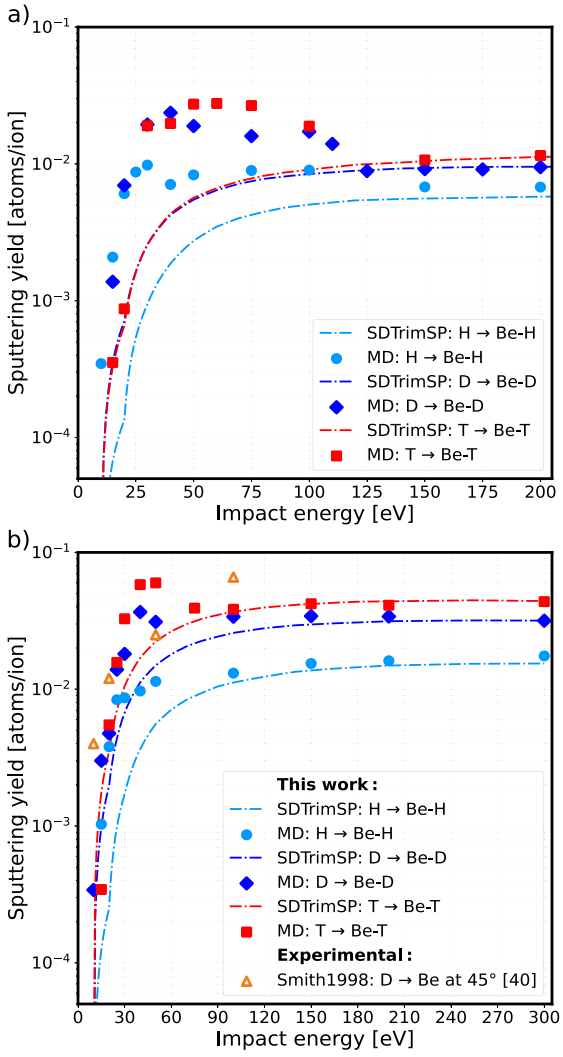


**Fig. 6.** Comparison of total sputtering yield by H, D, and T irradiations at 300 K for a) normal and b) 40° incidence. The experimental values are taken from Smith1998 [40].

### 3.1.2. Incident angle

The angle of incidence of the impinging ion significantly influences the level of erosion of PFCs. As shown in Fig. 7, increasing the incident angle from 0 to 65 degrees (with respect to the normal of the surface) will increase the sputtering yield exponentially.

This is caused by the shift in the primary mechanism responsible for sputtering from mode II to mode I. In mode II, sputtering occurs by a backscattered ion returning from the target's bulk to the surface, while in mode I, the projectile triggers sputtering immediately upon entering the surface layer of the target [41]. Consequently, the sputtering yield would be the sum of these two components. Since the first mechanism is much more effective than the second one, moving from 0 degrees, the yield increases until it reaches its maximum at approximately 65 degrees. However, a further increase in the impact angle will greatly increase the probability of reflection of the projectile from the surface to more than 65% (see the middle plots in Fig. S5), hence lowering the sputtering yield by reducing the number of projectiles entering the surface layer.

In contrast, in SDTrimSP, the maximum yield occurs at a higher angle of 75 degrees, and its value is lower than that of MD for all isotopes. Furthermore, once the peak yield is achieved, the reduction in yield is more pronounced in MD compared to SDTrimSP. The lower sputtering yield of SDTrimSP is not solely due to molecular sputtering, as physical

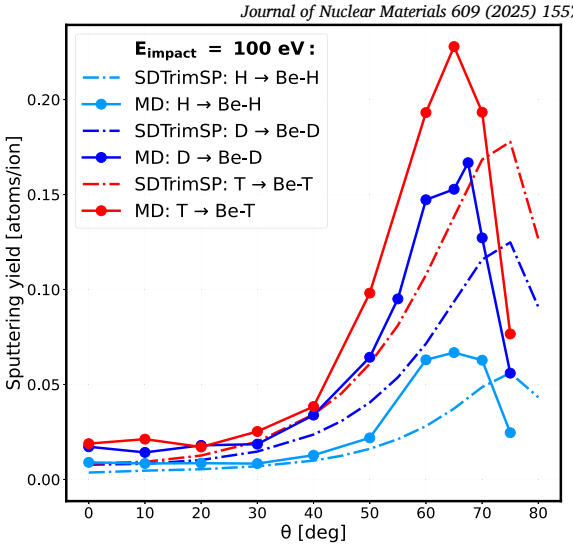


**Fig. 7.** Effect of incident angle on the sputtering yield at 300 K for impact energy of 100 eV.

sputtering predominates at these energy and impact angles. Additional factors, such as variations in target structures (with MD using a crystalline structure and SDTrimSP employing an amorphous one) might also play a role. A detailed investigation is required to pinpoint the source of this disparity, but such a study is beyond the scope of the current work.

### 3.1.3. Surface temperature

In this study, we primarily investigate the effect of surface temperature by focusing on the different hydrogen isotope concentration in the surface layer (Fig. 3), as other thermal effects on sputtering are low within the MD timescale. Fig. 8 shows the effect of surface temperature on the total Be sputtering yield. Our results indicate that there is no clear effect on the total Be sputtering yield in all structures. In contrast, surface temperature has a slightly more profound effect on CAPS and the types of sputtered molecules, which will be discussed in detail in the following section.

## 3.2. CAPS

As indicated above, molecular sputtering plays an important role in the erosion of Be surfaces, especially at low impact energies. In our MD simulations, the identification of molecular sputtering is based on the potential energy of the sputtered species along with their spatial distance. As an example, if the potential energy between a sputtered Be atom and a D atom is negative, and their distance remains around the typical bond length of a BeD molecule (1.34 Å) during the entire simulation, it can be concluded that a BeD molecule has been sputtered (refer to Fig. S6 for all the molecules identified in our simulations).

Fig. 9 shows the proportion of Be atoms sputtered as molecules in all structures for two impact angles. Our results verify the significant dependence of molecular sputtering on the projectile energy and mass. As the impact energy increases, the ratio of the sputtered molecules to the total sputtered species decreases exponentially. Initially, 100% of the Be atoms are sputtered as molecules at impact energies lower than 20 eV, but this decreases to about 10% at 150 eV. Moreover, the lighter the isotope is, the larger is the fraction of sputtered molecules in the mid-energy range.

We attribute this isotope effect to the difference in the momentum of the plasma particles. The momentum, $p$, can be calculated as $\sqrt{2Km}$, where $K$ is the kinetic energy of the projectile and $m$ is its mass. Therefore, for the same kinetic energy, the momentum of H will be approximately $\sqrt{2}$ and $\sqrt{3}$ times lower than that of D and T, respectively. The

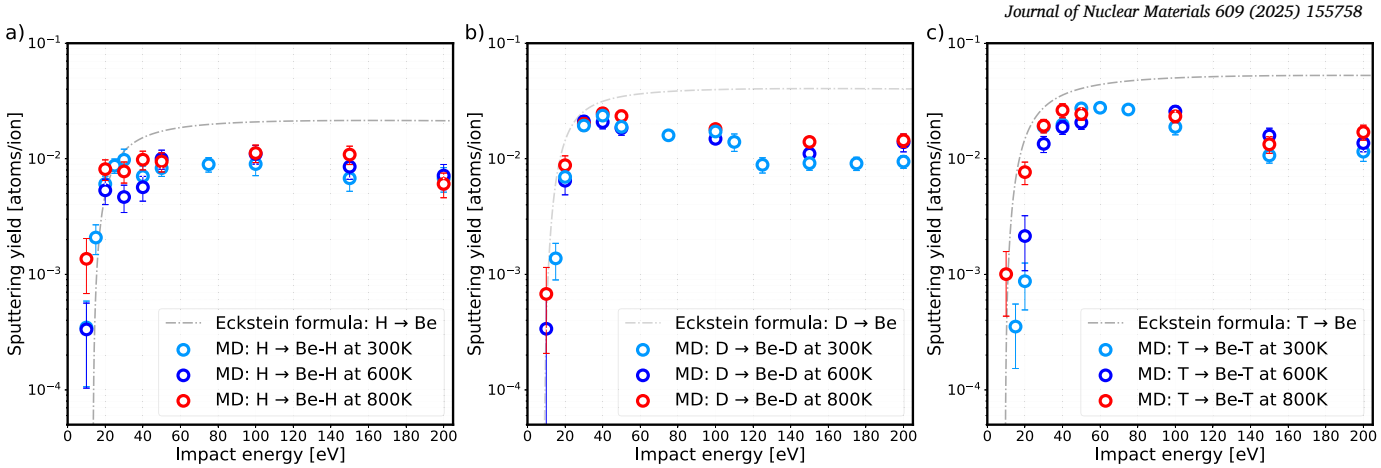


**Fig. 8.** Effect of surface temperature on the sputtering yield in a) Be-H, b) Be-D, and c) Be-T surfaces.

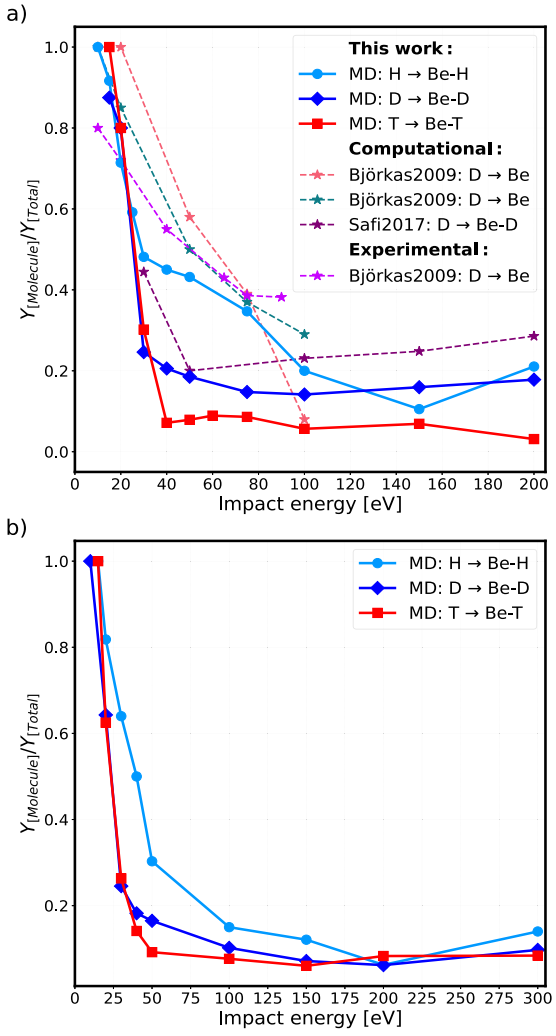


**Fig. 9.** The fraction of Be atoms eroded as molecules as a function of impact energy at 300 K for a) normal and b) 40° incidence.

increase in momentum, along with the more efficient momentum transfer as the mass of the isotope increases, results in a much higher physical sputtering. As a result, H exhibits the highest proportion of sputtered molecules, with D and T trailing behind. However, at impact energies higher than 100 eV, even though the momentum of H ions is still lower than that of the other two, it is still high enough to reduce the ratio of sputtered molecules due to the increased physical sputtering. Moreover, for the same impact energy, the lighter isotope will have a higher velocity, resulting in a shorter interaction time within the bonding region. Consequently, the energy interval in which the lighter isotope may induce CAPS is reduced compared to that of the heavier isotope (Fig. S7, panel a). Therefore, beyond this energy interval, the heavier isotope is more likely to cause CAPS and exhibit more molecular sputtering (Fig. S7, panel b), thus further decreasing the gap in the ratio of sputtered molecules between the isotopes.

Fig. 10 illustrates the effect of surface temperature on the molecular sputtering yield. In the Be-H surface (Fig. 10, panel a), for impact energies above 25 eV, the molecular yield is higher at 300 K compared to 600 and 800 K. The same trend can be seen for D ions (Fig. 10, panels b) with impact energies exceeding 50 eV. This result is in good agreement with the measurements from limiter discharges which have been carried out in the JET tokamak [42]. There, molecular sputtering from 75 eV D ions impacting a Be surface was seen to decrease with higher surface temperatures. For T (Fig. 10, panels c), we see a similar trend for impact energies exceeding 80 eV, although the effect for T is weak.

We attribute this behavior to the tendency of sputtered molecules to consist of a Be atom bonded to an H isotope originating from the surface, as observed in our simulations at 300 K. In the case of H, for impact energies greater than 25 eV, over 40% of the sputtered molecules consist of Be atoms bonded to H atoms originating from the hydrogenated surface layer (Fig. S8), and this fraction further increases with increasing impact energy. Consequently, at elevated surface temperatures, where the concentration of H atoms in the surface is substantially decreased, we observe a lower molecular sputtering at these impact energies. Similarly, in the cases of D and T, the fraction of sputtered molecules containing D or T atoms originating from the surface layer reaches 40% for impact energies above 50 eV and 80 eV, respectively (Fig. S8). Below these energies, most of the sputtered molecules contain the projectile. We find that the effect of increased surface temperature for these lower impact energies is the opposite, displaying higher molecular sputtering yields at higher surface temperatures, despite the decreasing hydrogen isotope content in the surface layer. Nevertheless, this does not contradict the agreement with the experimental observation [42], which was obtained for D impact energies well above 50 eV.

Moreover, we observe that the molecular sputtering exhibits no apparent sensitivity to structural imperfections due to vacancies. This is evident from the comparable molecular yield between the pristine Be surface at 300 K and the Be-D surface at 800 K (which has 7% vacancies and no D content), especially in the range of 100 to 200 eV (Fig. 10, panel b), where we have higher statistics (see Table 3). This further con-

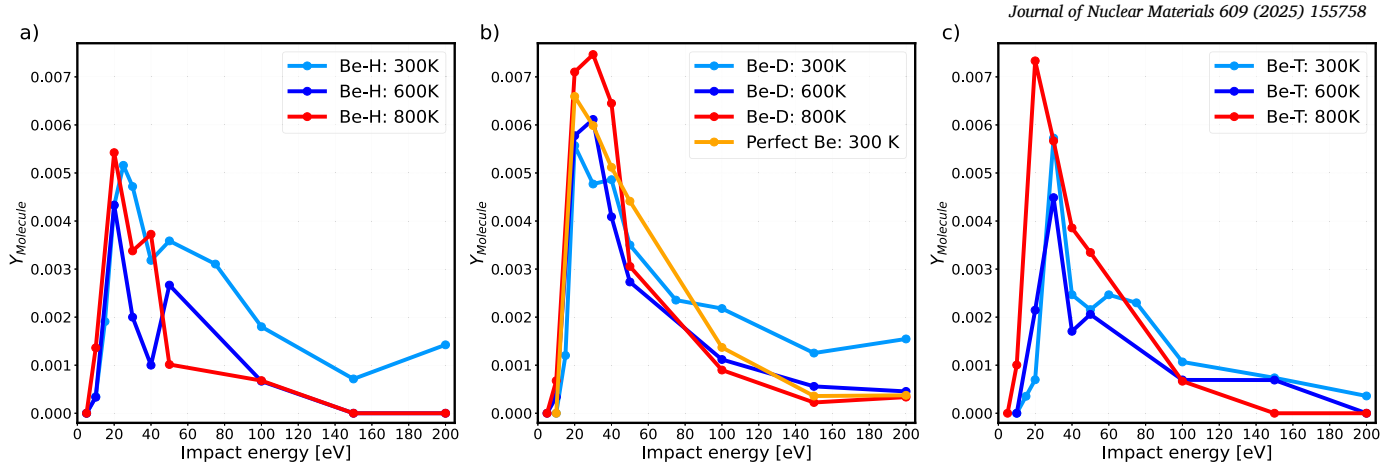


**Fig. 10.** Effect of surface temperature on molecular sputtering yield in a) Be-H, b) Be-D and perfect Be, and c) Be-T surfaces.

firms that the higher molecular sputtering yield observed in the Be-D structure at 300 K relative to the pristine Be within this energy interval (100 - 200 eV) is due solely to the presence of D atoms in the surface layer.

We note that in each structure, more than 92% of the sputtered molecules at 300 K are composed of BeH, BeD, or BeT molecules. Moving to 600 K, BeH and BeT are the only sputtered molecules in the corresponding structures, indicating the effect of hydrogen isotope concentration on the type of sputtered molecules. However, in the Be-D structure at 600 K, $BeD_2$ molecule still represents 1.5% of the total sputtered molecules (Fig. S6). It is worth noting that the majority of molecules observed in our MD simulations are also detected experimentally [43], lending confidence in the predictions of the interatomic potential. Exceptions are the $BeX_2$ and $BeX_3$ molecules observed in simulations, where X represents a hydrogen isotope. These particular molecules, however, would be unstable and would break down into other molecules when they reach the plasma, thus preventing direct spectroscopic access in experiments [42,44].

Finally, the angle of incidence can also influence the ratio of sputtered Be bound in molecules to the total Be yield. Our results indicate that an increase in impact angle leads to a lower ratio (Fig. S9, panel c). This is due to the rapid rise in physical sputtering, which is dramatically more pronounced—by a factor of ten—compared to the increase in molecular sputtering (Fig. S9, panels a and b). However, this relative reduction in CAPS is more pronounced in the Be-H structure and becomes less noticeable as the mass of the projectile increases.

### 3.3. Energy and angular distributions of sputtered species

Fig. 11 summarizes the energy and polar angle distribution of the sputtered species and their dependence on impact energy and incident angle, respectively. The energy distribution is broad for low impact energies and narrows as the projectile's energy increases. Moreover, the maximum of the energy distribution moves to higher energies, ranging from approximately 2 eV at an $E_{impact}$ of 30 eV to approximately 4 eV at an $E_{impact}$ of 200 eV. Similar results have been observed by S. Shermukhamedov et al. in MD simulations of a pure Be structure [45]. Furthermore, the energy distributions obtained by MD and SDTrimSP agree well with each other. In contrast, the agreement is less satisfactory for the polar angle distributions of the sputtered species. In both MD and SDTrimSP profiles, the peak of the distribution moves to higher angles by increasing the impact angle. However, SDTrimSP profiles are broader than those of MD, demonstrating a clearer influence of the impact angle on the distribution, potentially attributed to better statistics. The peaks in the MD profiles are more distinct, shifting from 45 degrees at a 10-degree incidence to 52 degrees at a 67.5-degree incidence. Nevertheless, achieving a more accurate comparison between MD and SDTrimSP results requires a considerably larger dataset for MD, which is resource-intensive. Overall, these findings indicate that the energy and angle of the sputtered species are strongly dependent on the properties of the projectile.

## 4. Conclusion

The focus of this work was to evaluate the sputtering of Be structures with different hydrogen isotope content and to determine the contribution of CAPS to erosion. This was achieved by conducting MD simulations that utilized both a small time step and variable cell size to ensure the accuracy of the results. This allowed us to capture the impact of molecular sputtering on total erosion and to determine the energy interval in which the predictions of MD differ significantly from those of BCA.

Our results show good agreement with the experimental sputtering yields of Be surfaces, particularly when D is present in the material. Furthermore, we demonstrate that SDTrimSP is unable to provide accurate data on sputtering at lower energies, where molecular sputtering contributes significantly to total erosion. This highlights the importance of performing MD simulations within this energy range to obtain more realistic and precise data on sputtering yields.

Moreover, we find a reduction in the ratio of the sputtered molecules to the total sputtered species as the mass of the projectile and angle of incidence increase, due to the increased physical sputtering. The surface temperature, or alternatively the concentration of hydrogen isotopes within the structure, does not exhibit a pronounced impact on the total sputtering yield. However, surface temperature has a more distinguishable effect on CAPS. For Be-H system from low impact energies, a higher molecular sputtering is detected at 300 K. In contrast, in Be-D and Be-T, molecular sputtering at 300 K is lower than at 800 K for low energies, but surpasses it as impact energy increases. This suggests that H behaves differently within the surface layers compared to D and T, affecting their contributions to CAPS.

Furthermore, both the SDTrimSP and MD findings suggest that increasing the impact energy and incident angle of the projectile shifts the peak of the energy and angle distribution of the sputtered species to higher values, respectively.

This work provides new insights into the effect of isotopes on chemically assisted physical sputtering mechanisms of plasma-wall erosion. We also provide an extensive high-fidelity dataset for lower particle impact energies that can be used as input for impurity transport codes such as ERO, significantly improving upon the accuracy obtainable by BCA methods. This will lead to a better understanding of PWIs and their effect on reactor performance.

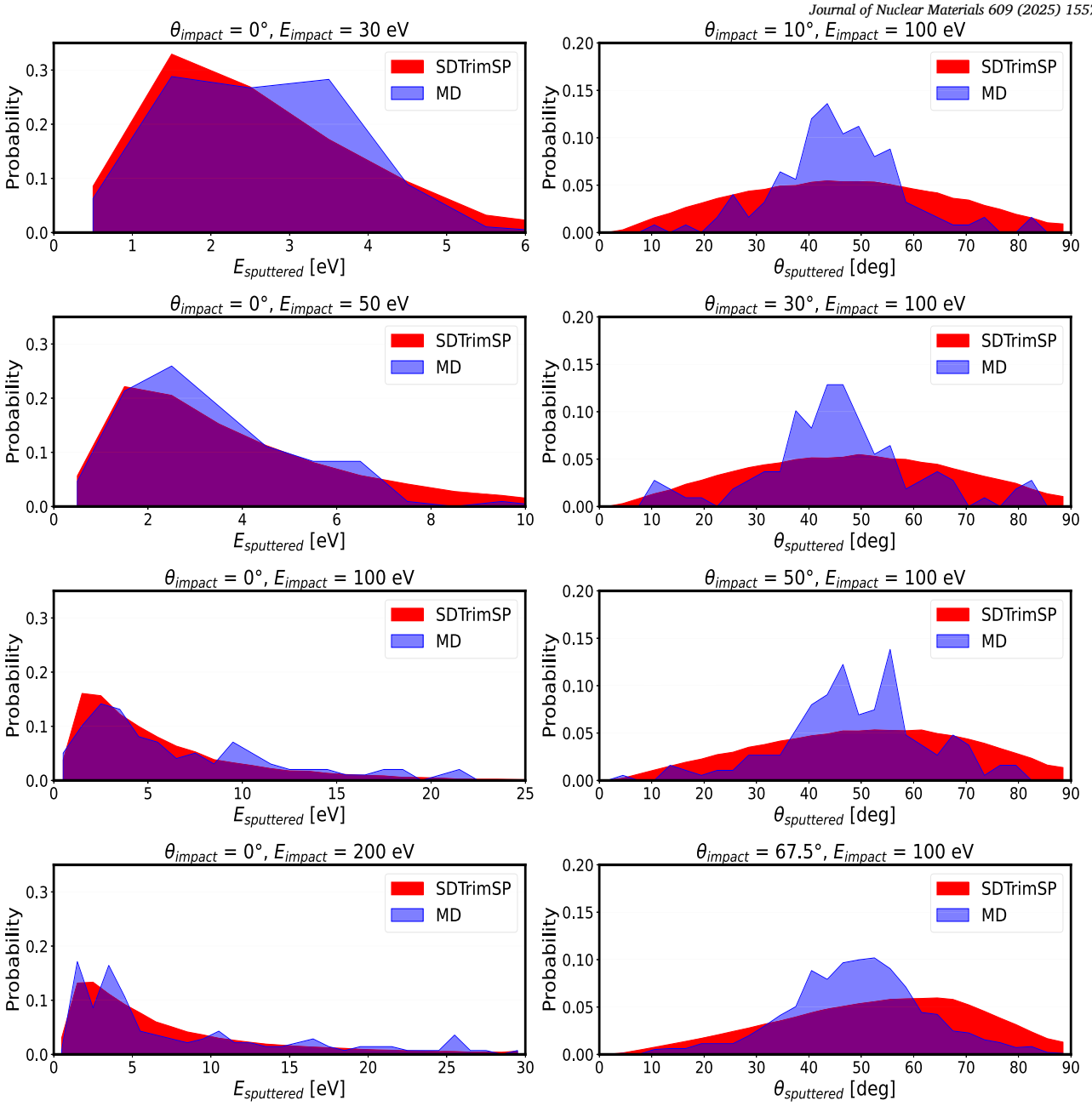


**Fig. 11.** Energy and angle distribution of sputtered species in Be-D structure.

## CRediT authorship contribution statement

**Nima Fakhrayi Mofrad:** Writing – review & editing, Writing – original draft, Visualization, Validation, Software, Methodology, Investigation, Formal analysis, Data curation. **Juri Romazanov:** Writing – review & editing, Visualization, Software, Conceptualization. **Roy Schumacher:** Visualization, Formal analysis, Data curation. **Andrea E. Sand:** Writing – review & editing, Validation, Supervision, Software, Resources, Project administration, Methodology, Investigation, Funding acquisition, Conceptualization.

## Supporting information available

One pdf file with additional figures and data analysis is available for download. The data required to reproduce these findings will be available upon reasonable request.

## Declaration of competing interest

The authors declare that they have no known competing financial interests or personal relationships that could have appeared to influence the work reported in this paper.

## Acknowledgements

The calculations presented above were performed using computer resources within the Aalto University School of Science “Science-IT” project. This work has been carried out within the framework of the EUROfusion Consortium, funded by the European Union via the Euratom Research and Training Programme (Grant Agreement No 101052200 - EUROfusion). Views and opinions expressed are, however, those of the authors only and do not necessarily reflect those of the European Union or the European Commission. Neither the European Union nor the European Commission can be held responsible for them.

## Appendix A. Supplementary material

Supplementary material related to this article can be found online at https://doi.org/10.1016/j.jnucmat.2025.155758.

## Data availability

Data will be made available on request.

## References

[1] J. Biener, et al., A surface reaction with atoms: hydrogenation of sp- and sp2-hybridized carbon by thermal H(D) atoms, J. Chem. Phys. (ISSN 0021-9606) 99 (4) (Aug. 1993) 3125–3128, https://doi.org/10.1063/1.465166.

[2] W. Jacob, Surface reactions during growth and erosion of hydrocarbon films, Thin Solid Films (ISSN 0040-6090) 326 (1) (1998) 1–42, https://doi.org/10.1016/S0040-6090(98)00497-0.

[3] Gregory De Temmerman, et al., Data on erosion and hydrogen fuel retention in Beryllium plasma-facing materials, Nucl. Mater. Energy (ISSN 2352-1791) 27 (2021) 100994, https://doi.org/10.1016/j.nme.2021.100994.

[4] K. Nordlund, et al., Multiscale modelling of plasma–wall interactions in fusion reactor conditions, J. Phys. D, Appl. Phys. 47 (22) (May 2014) 224018, https://doi.org/10.1088/0022-3727/47/22/224018.

[5] Peter Sigmund, Theory of sputtering. I. Sputtering yield of amorphous and polycrystalline targets, Phys. Rev. 184 (Aug. 1969) 383–416, https://doi.org/10.1103/PhysRev.184.383.

[6] Rainer Behrisch, Wolfgang Eckstein, Sputtering by Particle Bombardment: Experiments and Computer Calculations from Threshold to MeV Energies, vol. 110, Springer Science & Business Media, 2007.

[7] W. Eckstein, J. Bohdansky, J. Roth, Physical sputtering, Nucl. Fusion 1 (1991) 51.

[8] J. Roth, C. Garcia-Rosales, Analytic description of the chemical erosion of graphite by hydrogen ions, Nucl. Fusion 36 (12) (1996) 1647.

[9] K. Nordlund, et al., Swift chemical sputtering of covalently bonded materials, Pure Appl. Chem. 78 (6) (2006) 1203–1211, https://doi.org/10.1351/pac200678061203.

[10] E. Salonen, et al., Bond-breaking mechanism of sputtering, Europhys. Lett. 52 (5) (Dec. 2000) 504, https://doi.org/10.1209/epl/i2000-00466-6.

[11] K. Nordlund, et al., Mechanism of swift chemical sputtering: comparison of Be/C/W dimer bond breaking, Nucl. Instrum. Methods Phys. Res., Sect. B, Beam Interact. Mater. Atoms (ISSN 0168-583X) 269 (11) (2011) 1257–1261, https://doi.org/10.1016/j.nimb.2010.12.080.

[12] C. Björkas, et al., Molecules can be sputtered also from pure metals: sputtering of beryllium hydride by fusion plasma–wall interactions, Plasma Phys. Control. Fusion 55 (7) (June 2013) 074004, https://doi.org/10.1088/0741-3335/55/7/074004.

[13] C. Björkas, et al., Chemical sputtering of Be due to D bombardment, New J. Phys. 11 (12) (Dec. 2009) 123017, https://doi.org/10.1088/1367-2630/11/12/123017.

[14] D. Borodin, et al., Improved ERO modelling of beryllium erosion at ITER upper first wall panel using JET-ILW and PISCES-B experience, Nucl. Mater. Energy (ISSN 2352-1791) 19 (2019) 510–515, https://doi.org/10.1016/j.nme.2019.03.016.

[15] E. de la Cal, et al., Measuring the isotope effect on the gross beryllium erosion in JET, Nucl. Fusion 62 (12) (Oct. 2022) 126021, https://doi.org/10.1088/1741-4326/ac8aae.

[16] J. Mailloux, et al., Overview of JET results for optimising ITER operation, Nucl. Fusion 62 (4) (June 2022) 042026, https://doi.org/10.1088/1741-4326/ac47b4.

[17] G. Federici, Plasma wall interactions in ITER, Phys. Scr. 2006 (T124) (Apr. 2006) 1, https://doi.org/10.1088/0031-8949/2006/T124/001.

[18] R.A. Pitts, et al., Plasma-wall interaction impact of the ITER re-baseline, Nucl. Mater. Energy (ISSN 2352-1791) 42 (2025) 101854, https://doi.org/10.1016/j.nme.2024.101854.

[19] A. Annen, A. von Keudell, W. Jacob, Erosion of amorphous hydrogenated boron-carbon thin films, J. Nucl. Mater. (ISSN 0022-3115) 231 (1) (1996) 151–154, https://doi.org/10.1016/0022-3115(96)00389-3.

[20] A. Annen, W. Jacob, Chemical erosion of amorphous hydrogenated boron films, Appl. Phys. Lett. 71 (10) (1997) 1326–1328.

[21] S. Brezinsek, et al., Chemically assisted physical sputtering of Tungsten: identification via the $6\Pi \rightarrow 6\Sigma^+$ transition of WD in TEXTOR and ASDEX Upgrade plasmas, Nucl. Mater. Energy (ISSN 2352-1791) 18 (2019) 50–55, https://doi.org/10.1016/j.nme.2018.12.004.

[22] A. Kirschner, et al., Modelling of impurity transport and plasma–wall interaction in fusion devices with the ERO code: basics of the code and examples of application, Contrib. Plasma Phys. 56 (6–8) (2016) 622–627.

[23] A.P. Thompson, et al., LAMMPS - a flexible simulation tool for particle-based materials modeling at the atomic, meso, and continuum scales, Comput. Phys. Commun. 271 (2022) 108171, https://doi.org/10.1016/j.cpc.2021.108171.

[24] C. Björkas, et al., Interatomic potentials for the Be-C-H system, J. Phys. Condens. Matter (ISSN 0953-8984) 21 (44) (2009), https://doi.org/10.1088/0953-8984/21/44/445002.

[25] E. Safi, et al., Multi-scale modelling to relate beryllium surface temperature, deuterium concentration and erosion in fusion reactor environment, J. Phys. D, Appl. Phys. (ISSN 1361-6463) 50 (Apr. 2017), https://doi.org/10.1088/1361-6463/aa6967.

[26] Pierre Hirel, Atomsk: a tool for manipulating and converting atomic data files, Comput. Phys. Commun. (ISSN 0010-4655) 197 (2015) 212–219, https://doi.org/10.1016/j.cpc.2015.07.012.

[27] Alexander Stukowski, Visualization and analysis of atomistic simulation data with OVITO–the Open Visualization Tool, Model. Simul. Mater. Sci. Eng. 18 (1) (Dec. 2009) 015012, https://doi.org/10.1088/0965-0393/18/1/015012.

[28] Herman J.C. Berendsen, et al., Molecular dynamics with coupling to an external bath, J. Chem. Phys. 81 (8) (1984) 3684–3690.

[29] Katharina Vörtler, Kai Nordlund, Molecular dynamics simulations of deuterium trapping and re-emission in tungsten carbide, J. Phys. Chem. C 114 (12) (2010) 5382–5390, https://doi.org/10.1021/jp9054473.

[30] Sangrak Kim, Issues on the choice of a proper time step in molecular dynamics, in: 26th Annual CSP Workshop on “Recent Developments in Computer Simulation Studies in Condensed Matter Physics”, CSP 2013, Phys. Proc. (ISSN 1875-3892) 53 (2014) 60–62, https://doi.org/10.1016/j.phpro.2014.06.027.

[31] James F. Ziegler, Jochen P. Biersack, The stopping and range of ions in matter, in: D. Allan Bromley (Ed.), Treatise on Heavy-Ion Science: Volume 6: Astrophysics, Chemistry, and Condensed Matter, Springer US, Boston, MA, ISBN 978-1-4615-8103-1, 1985, pp. 93–129.

[32] W. Möller, W. Eckstein, Tridyn — a TRIM simulation code including dynamic composition changes, Nucl. Instrum. Methods Phys. Res., Sect. B, Beam Interact. Mater. Atoms (ISSN 0168-583X) 2 (1) (1984) 814–818, https://doi.org/10.1016/0168-583X(84)90321-5.

[33] A. Mutzke, et al., SDTrimSP Version 6.00, Max-Planck-Institut für Plasmaphysik, Garching, 2019.

[34] W.D. Wilson, L.G. Haggmark, J.P. Biersack, Calculations of nuclear stopping, ranges, and straggling in the low-energy region, Phys. Rev. B 15 (Mar. 1977) 2458–2468, https://doi.org/10.1103/PhysRevB.15.2458.

[35] A. Mutzke, G. Bandelow, R. Schneider, Sputtering of mixed materials of beryllium and tungsten by hydrogen and helium, J. Nucl. Mater. (ISSN 0022-3115) 467 (2015) 413–417, https://doi.org/10.1016/j.jnucmat.2015.05.052.

[36] D. Nishijima, et al., Erosion yields of deposited beryllium layers, in: Proceedings of the 18th International Conference on Plasma-Surface Interactions in Controlled Fusion Device, J. Nucl. Mater. (ISSN 0022-3115) 390–391 (2009) 132–135, https://doi.org/10.1016/j.jnucmat.2009.01.144.

[37] Shokirbek Shermukhamedov, et al., Modelling the sputtering and reflection from a beryllium surface: atomistic analysis, Nucl. Fusion 61 (8) (June 2021) 086013, https://doi.org/10.1088/1741-4326/ac044e.

[38] Joachim Roth, Wolfgang Eckstein, Maria Guseva, Erosion of Be as plasma-facing material, Fusion Eng. Des. (ISSN 0920-3796) 37 (4) (1997) 465–480, https://doi.org/10.1016/S0920-3796(97)00091-4.

[39] A. Lasa, et al., MD simulations of low energy deuterium irradiation on W, WC and W2C surfaces, J. Nucl. Mater. 429 (1–3) (2012) 284–292.

[40] P.C. Smith, D.N. Ruzic, Low energy (10 to 700 eV) angularly resolved sputtering yields for $D^+$ on beryllium, Nucl. Fusion 38 (5) (May 1998) 673, https://doi.org/10.1088/0029-5515/38/5/303.

[41] R. Weissmann, R. Behrisch, Contributions of backscattered ions to sputtering yields depending on primary ion energy, Radiat. Eff. 19 (2) (1973) 69–75, https://doi.org/10.1080/00337577308232221.

[42] S. Brezinsek, et al., Study of physical and chemical assisted physical sputtering of beryllium in the JET ITER-like wall, Nucl. Fusion 54 (10) (Sept. 2014) 103001, https://doi.org/10.1088/0029-5515/54/10/103001.

[43] Felix Duensing, et al., Energetic D+ and He+ impinging on solid beryllium: observation of physical and chemically assisted atomic and molecular ion sputtering, Nucl. Mater. Energy (ISSN 2352-1791) 30 (2022) 101110, https://doi.org/10.1016/j.nme.2021.101110.

[44] E. Safi, et al., Atomistic simulations of the effect of reactor-relevant parameters on be sputtering, J. Nucl. Mater. (ISSN 0022-3115) 463 (2015) 805–809, https://doi.org/10.1016/j.jnucmat.2014.10.050.

[45] S. Shermukhamedov, et al., Sputtering and reflection from a beryllium surface: effects of hydrogen isotope mass, impact position and surface binding energy, Nucl. Fusion 62 (6) (Apr. 2022) 066024, https://doi.org/10.1088/1741-4326/ac592a.